Charge Transport through Polyene Self-Assembled Monolayers from Multiscale Computer Simulations

Christopher George, Hidehiro Yoshida, and William A. Goddard III*

Materials and Process Simulation Center (139-74), California Institute of Technology, Pasadena, California, 91125

Seung Soon Jang

School of Materials Science and Engineering, Georgia Institute of Technology, Atlanta, Georgia 30332-0245

Yong-Hoon Kim*

Department of Materials Science and Engineering, University of Seoul, 90 Jeonnong-dong, Dongdaemun-gu, Seoul, 130-743 Korea

Received: March 21, 2006; Revised Manuscript Received: July 9, 2008

We combine first-principles density-functional theory with matrix Green's function calculations to predict the structures and charge transport characteristics of self-assembled monolayers (SAMs) of four classes of systems in contact with Au(111) electrodes: conjugated polyene chains ($n = 4$, 8, 12, 16, and 30) thiolated at one or both ends and saturated alkane chains ($n = 4$, 8, 12, and 16) thiolated at one or both ends. **For the polyene SAMs, we find no decay in the current as a function of chain length and conclude that these 1−3 nm long polyene SAMs act as metallic wires.** We also find that the polyene-monothiolate leads to a contact resistance only 2.8 times higher than that for the polyene-dithiolate chains, indicating that the device conductance is dominated by the properties of the molecular connector with less importance in having a second molecule−electrode contact. For the alkane SAMs, we observe the normal exponential decay in the current as a function of the chain length with a decay constant of $\beta_n = 0.82$ for the alkane-monothiolate and 0.88 for the alkane-dithiolate. We find that the contact resistance for the alkane-monothiolate is 12.5 times higher than that for the alkane-dithiolate chains, reflecting the extra resistance due to the weak contact on the nonthiolated end. These contrasting charge transport characteristics of alkane and polyene SAMs and their contact dependence are explained in terms of the atomic projected density of states.

1. Introduction

Recent advances in molecular electronics are leading to novel candidates for future miniaturization of electronic devices.[1,2] These applications depend sensitively on the charge transport behavior of the molecular-based systems connected to the electrodes in the nanometer scale. Progress is hampered because device structures having precise configuration and composition are difficult to synthesize and characterize. This situation makes computational studies highly valuable.

We present here a first-principles study of the charge transport properties for four classes of self-assembled monolayers (SAMs) sandwiched between Au(111) electrodes.

- *trans-n*-alkane-monothiolate: Au−S$(CH_2)_{n-1}CH_3$···Au with $n = 4$, 8, 12, and 16 (Figure 1a)
- *trans-n*-alkane-dithiolate: Au−S$(CH_2)_n$S−Au with $n = 4$, 8, 12, and 16 (Figure 1b)
- *trans-n*-polyene-monothiolate: Au−S$(CH)_{n-1}$−CH_2···Au with $n = 4$, 8, 12, 16, and 30 (Figure 1c)
- *trans-n*-polyene-dithiolate Au−S$(CH)_n$S−Au with $n = 4$, 8, 12, 16, and 30 (Figure 1d)

These studies use a multiscale computational approach that combines quantum mechanical (QM) density-functional theory (DFT) and matrix Green's function (MGF) calculations with classical force-field (FF) molecular dynamics (MD) simulations.[3−7] We expect that such SAMs will be advantageous for device applications, because the intermolecular interactions in the SAM provides a more stable and reproducible structure than isolated single molecules.[8] This should simplify synthesis and should yield the more consistent performance required for practical device applications.

We find that the SAMs based on the *n*-polyene chains lead to a conductance that is nearly independent of the chain length, even up to $n = 30$. This indicates that the nanoscale polyene SAM behaves more like a metal. In contrast, we find that *n*-alkane-thiolate and *n*-alkane-dithiolate chains exhibit the more common exponential decay in the conductance with respect to the chain length, in agreement with previous experimental and theoretical studies.

We also determined the differential contact resistance between having the chain covalently attached to the Au surface through thiolates at both ends (C−S−Au) versus leaving one of the chain ends with a van der Waals contact to the Au surface (CH_3···Au for the alkanethiolates and CH_2···Au for the polyenethiolates). For the alkane-dithiolate SAM, we find that its conductance is larger than its monothiolate counterpart by a factor of about 12, showing that the device conductance is dominated by the molecule−electrode contacts for the alkane-based SAMs. In contrast, we find that the contact resistance for *n*-polyene-dithiolate chains is only 2.8 times smaller than that for their

* To whom correspondence may be addressed. E-mail: wag@wag.caltech.edu (W.A.G.); y.h.kim@uos.ac.kr (Y.-H.K.).

10.1021/jp061759l CCC: $40.75
Published on Web 10/24/2008

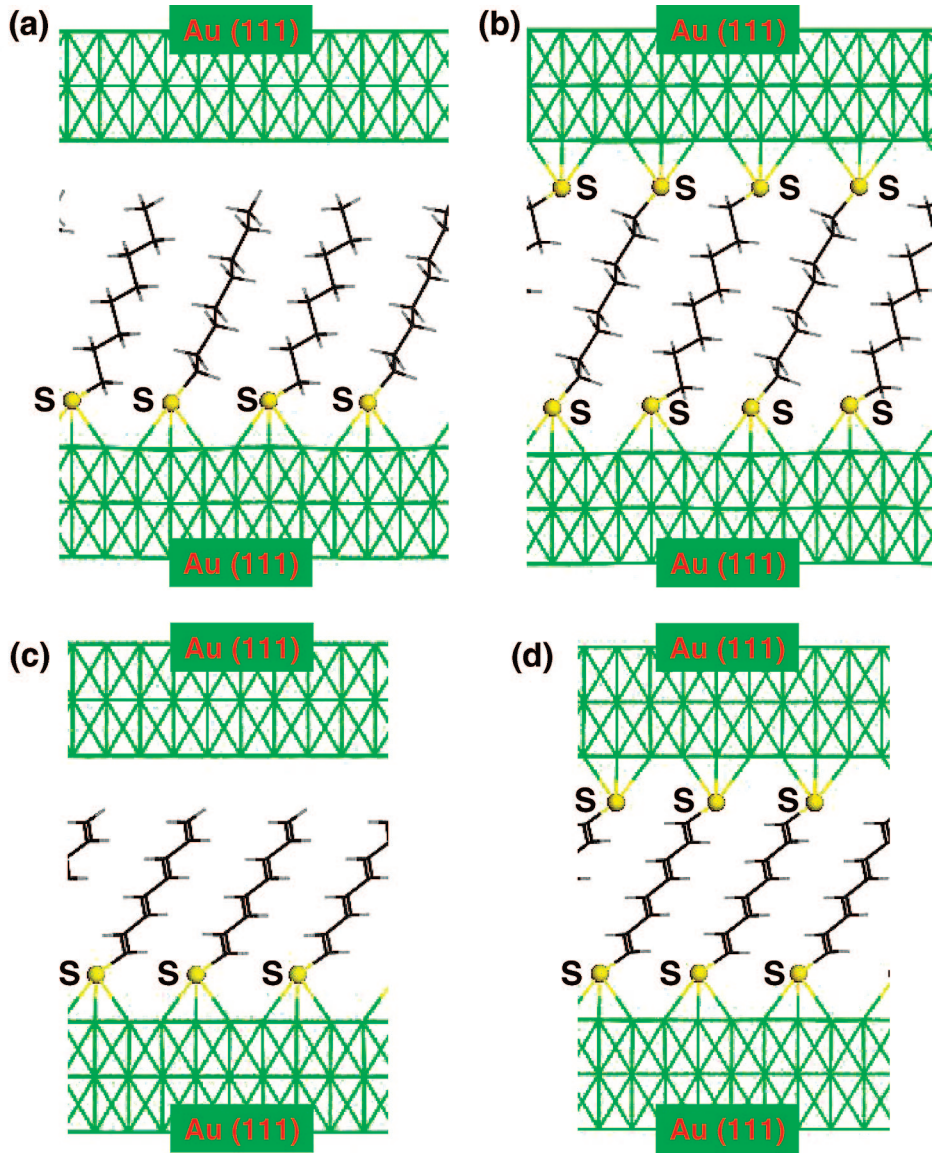

Figure 1. Configurations of the molecular electronic devices considered in this work: (a) alkane-thiolate, (b) alkane-dithiolate, (c) polyene-thiolate, and (d) polyene-dithiolate SAMs. 8-Alkane and 8-polyene cases are shown. All geometric variables were optimized within the FF.

monothiolate counterparts. This indicates that the polyene SAM device conductance is determined by the properties of the molecular connector with less importance in having a second molecule−electrode contact.

The contrasting charge transport behavior of the alkane and polyene SAMs as well as their contact dependence will be explained via projected density of states (PDOS) of molecular cores and thiolate bridges.

2. Monolayer and Device Structures from FF Molecular Dynamics and Energy Minimization

The structural properties of these SAMs were described using two-dimensional (2D) periodic boundary conditions based on the Dreiding FF[9] modified by including extra interaction terms between the S and the Au surface based on DFT calculations of $S-CH_2-CH_3$ bonded to an Au_{28} cluster.[10] Charges were obtained using the charge equilibration model.[11] A more detailed description of the procedure was described previously.[3]

2.1. Alkane Case. To obtain the optimum packing and structure for the *n*-alkane(mono)thiolate SAMs, we considered the 12-alkane-thiolates $[S-(CH_2)_{11}-CH_3]$ on a 2D Au(111) periodic slab consisting of four atomic layers. It is well-known that *n*-alkane-thiolates ($n \geq 6$) form well-ordered SAMs on the Au(111) surface at the packing density $(\sqrt{3} \times \sqrt{3})R30°$ and molecule tilt angle of about 30° from the surface normal direction.[8] To find out the optimal packing density, we employed the 1×1, 2×1, $\sqrt{3} \times \sqrt{3}$, 2×2, 3×2, and 3×3 Au unit cells (1, 2, 3, 4, 6, and 9 Au atoms in one atomic layer) per chain within the 2D periodic boundary condition, as shown in Figure 2.

Using this SAM model, we performed MD simulations at 300 K using the Nose−Hoover thermostat (*NVT*) for 1−2 ps (MD time steps of 1.0 fs), allowing the system to relax. These structures were then energy minimized. To check the reliability of our results and the effect of superstructure formation, we doubled the unit cell to contain two independent chains. The cohesive energy or formation energy was calculated using the equation

$$\text{Energy}_{\text{Formation}} = \frac{\text{Energy}_{\text{Total}} - (\text{Energy}_{\text{Gold}} + N \times \textit{Energy}_{\textit{Molecule}})}{N} \quad (1)$$

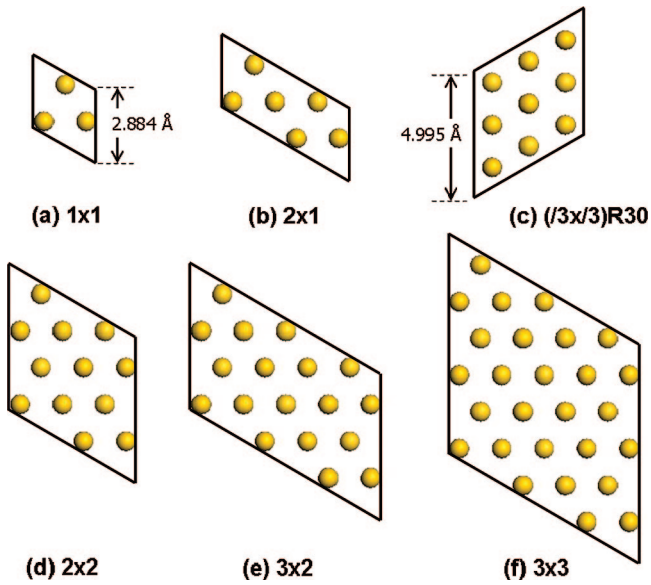

Figure 2. Top view of (a) 1 × 1, (b) 2 × 1, (c) ($\sqrt{3} \times \sqrt{3}$)R30°, (d) 2 × 2, (e) 3 × 2, and (f) 3 × 3 Au 1 × 1 unit cells. The number of Au atoms per layer is 1, 2, 3, 4, 6, and 9, respectively.

where $N = 1$ for the single chain and $N = 2$ for the double chains. The results are listed in Table 1.

We find that the optimum coverage for the alkane-thiolate case has a packing of one molecule per 3 gold atoms in one atomic layer [9 Au atoms in one Au(111) unit cell], which corresponds to the ($\sqrt{3} \times \sqrt{3}$)R30° packing observed experimentally. The energy-minimized 12-alkane-thiolate SAM conformation for the ($2\sqrt{3} \times \sqrt{3}$)R30° cell is shown in Figure 3a. This ($2\sqrt{3} \times \sqrt{3}$)R30° superstructure leads to a herringbone pattern with the S atoms at the 3-fold face-centered cubic (FCC) hollow site. We calculate a final angle of the chains with respect to the surface of 34.1 ± 0.5°, which agrees with the experimental values of 30°,[12] 34°,[13] and 34°,[14] and previous calculations of 28.3°[15] and 25−34°.[16]

Within the packing density of one thiolate per three surface Au atoms, S adsorption sites and the actual superstructure remains in dispute. Some studies[15,17] proposed the formation of a disulfide bond on the Au(111) surface, while others[18] have argued against the disulfide bond formation. Later, it was suggested that both may coexist.[19] More recent experiments find a new SAM structural model in which pairs of thiolates are bound to a bridging Au adatom above the ideal (111) surface.[20,21]

Regarding the superstructure, there is evidence suggesting that the dominant superlattice structure is c(4 × 2), including 8 molecules [equivalent to the (3 × $2\sqrt{3}$)rect superstructure that includes four molecules] with no disulfide bond.[8,22,23] However, experiments also find that the c(4 × 2) phase can coexist with the ($\sqrt{3} \times \sqrt{3}$)R30° phase.[14,17,24]

As mentioned above, more recent studies have observed thiolates bound to bridging Au adatoms.[20,21,25] However, we will limit ourselves here to the idealized Au(111) surface. In this case, theoretical studies report that the energetic difference between the ($\sqrt{3} \times \sqrt{3}$)R30° phase with one chain per unit cell and c(4 × 2) phase with four chains per unit cell is negligible (about 0.5−1 kcal/mol difference):[18,19] Our FF predicts that the c(4 × 2) configuration is a stable local energy minimum structure, and the ($2\sqrt{3} \times \sqrt{3}$)R30° herringbone configuration is 1.35 kcal/mol per molecule more stable than the c(4 × 2) configuration and 1.49 kcal/mol per molecule more stable than the ($\sqrt{3} \times \sqrt{3}$)R30° parallel configuration (leading to the global energy minimum). We calculated that the tilt angle for each packing model is very similar: 33.39° for ($\sqrt{3} \times \sqrt{3}$)R30°, 33.29° for c(4 × 2), and 33.20° for ($2\sqrt{3} \times \sqrt{3}$)R30°. Since this energy difference is small compared to kT and since such differences in monolayer packing (with the same tilt angle) have only negligible effects on the charge transport characteristics of alkane SAMs,[4] we use the simpler ($2\sqrt{3} \times \sqrt{3}$)R30° superstructure for all QM calculations of charge transport.

To prepare device models for the QM calculations, we repeated the above procedures of FF MD and energy minimization for the 4-, 8-, and 16-alkane-thiolate SAMs packed into the ($2\sqrt{3} \times \sqrt{3}$)R30° unit cell. We then capped the 4-, 8-, 12-, and 16-alkane SAMs with the top Au(111) electrodes. We considered both monothiolate and dithiolate junctions and included three atomic layers in the bottom and top electrodes. For the dithiolate SAM models, we carried out additional *NVT* MD simulations with the top electrode allowed to float down in the vacuum above the organic chains. This final structure had the top sulfur atoms binding to the top electrode in the 3-fold FCC hollow sites, just as for the bottom S−Au junctions. The system was then energy minimized to obtain the structure to be used in calculating charge transport properties. The device geometry for the 12-alkane-dithiolate junction is shown in Figure 4a.

For the monothiolate device models, the top S atoms of the dithiolate device models were replaced by H atoms and the structures were energy minimized within FF. For the 12-alkane-thiolate case, this leads to the structure shown in Figure 4b.

2.2. Polyene Case. For the polyene case, we used the same procedure as for the alkanes. We considered only the all-*trans* polyenes. To obtain the optimum SAM packing density, we employed the 12-polyene-monothiolate on a 2D Au(111) slab with four atomic layers. We calculated the cohesive energies for the 1 × 1, 2 × 1, $\sqrt{3} \times \sqrt{3}$, 2 × 2, 3 × 2, and 3 × 3 Au unit cells using single and double chain cases as in the alkane case. The results are listed in Table 2.

We find that the optimum coverage for the polyene-thiolates has a packing density of ($\sqrt{3} \times \sqrt{3}$)R30° just as in the alkane-thiolate case. On the other hand, the tilt angle is 48°, much larger than the 34° found for the alkane SAMs. The geometry of the 12-polyene-thiolate SAM in the ($2\sqrt{3} \times \sqrt{3}$)R30° cell is shown in Figure 3b. The polyene chains were found to lie parallel to one another with S atoms bonded to the Au surface at the FCC hollow sites, which corresponds to a ($\sqrt{3} \times \sqrt{3}$)R30° unit-cell superstructure. This configuration was also checked using the 3 × 3 ($\sqrt{3} \times \sqrt{3}$)R30° supercell (with an area of 195 Å^2) including nine organic chains on the cell surface.

Experimental realizations of nanoscale all-*trans* polyene junctions have not yet been reported. For the bulk polyacetylene, it was possible to obtain 81% crystallinity with 97% *trans* content.[26] These numbers vary depending on annealing time and temperature but do not approach perfect crystallinity with 100% *trans* content. Achieving well-ordered polyene SAMs is even more difficult because they oxidized readily when a bias voltage is applied to the Au electrodes. Thus, our data based on perfectly crystalline polyene SAM structures with 100% *trans* content cannot yet be directly compared with experiments.

After determining the SAM structures for the *n*-polyene-thiolates with $n = 4$, 8, 12, 16, and 30 at the optimal ($\sqrt{3} \times \sqrt{3}$)R30° packing density, we prepared device models for the calculations of charge transport properties. Although the ($\sqrt{3} \times \sqrt{3}$)R30° unit cell was found to be the optimal superstructure for the *n*-polyenes, we employed the ($2\sqrt{3} \times \sqrt{3}$)R30° unit cell as for the alkane case for the numerical consistency. The

TABLE 1: Tilt Angles and Formation Energies of 12-Alkane-thiolate SAMs for Various Packing Densities

system	number of surface Au atoms/chain	area per molecule (Å^2)	tilt angle (deg)	total energy (kcal/mol)	energy of gold (kcal/mol)	energy of molecule (kcal/mol)	formation energy (kcal/mol)
single 12-alkane chain	2	14.41	31.7	−23.43	−172.39	12.46	136.49
	3	21.61	**35.4**	−307.90	−252.63	12.46	**−67.73**
	4	28.81	49.8	−384.96	−344.83	12.46	−52.59
	6	43.22	67.0	−552.00	−517.29	12.46	−47.17
	9	64.83	77.4	−804.68	−775.91	12.46	−41.23
double 12-alkane chains	1	14.41	0	1187.21	−172.39	12.46	667.34
	2	28.81	14.3	−215.19	−344.83	12.46	52.36
	3	43.21	**35.1**	−606.68	−507.59	12.46	**−62.00**
	4	57.63	52.1	−766.47	−689.70	12.46	−50.85
	6	86.44	57.5	−1087.04	−1031.25	12.46	−40.35

n-polyene-dithiolate structures were energy minimized after *NVT* FF MD simulations with the top electrode being allowed to float down in a vacuum above the organic chains. Both the bottom and top sulfur atoms were found to prefer the 3-fold FCC hollow sites on the Au surface. Finally, the system was energy minimized, giving the device structures as shown in Figure 4c and d for the 12-polyene case. Finally, we started with the FF-derived device structures and performed additional DFT QM energy minimizations for the molecular structures, while fixing the Au(111) electrodes (see section 3 for the DFT computational details).

3. Confirmation of the $(\sqrt{3} \times \sqrt{3})$R30° Packing Density Using Density-Functional Calculations

Starting with the 8-alkane-thiolate and 8-polyene-thiolate SAM structures energy minimized within the FF, we used the **SEQQUEST**[27] program to perform 2D (slab geometry) DFT calculations to validate the accuracy of the FF studies. We considered here the 8-alkane/polyene-thiolate SAMs with the $1 \times 1(2 \times 1)$, $1 \times 1(\sqrt{3} \times \sqrt{3})$R30°, and $1 \times 1(2 \times 2)$ Au cells each with three Au(111) substrate layers. We used the Perdew−Burke−Ernzerhof (PBE) parametrization of generalized-gradient approximation (GGA),[28] with norm-conserving scalar-relativistic pseudopotentials to remove the core electrons.[29] The Kohn−Sham orbitals were expanded in terms of the double-ζ-polarization quality Gaussian basis set optimized for the corresponding pseudopotentials. The exchange-correlation energy and Hartree potential were calculated using a uniform real-space grid with 0.3 Bohr spacing. For the *k*-space sampling, we used shifted 2×4, 2×2, and 2×2 interface-parallel reciprocal $\vec{k}_{||}$ points for the energy minimization of 2×1, $(\sqrt{3} \times \sqrt{3})$R30°, and 2×2 Au unit cells, respectively, and 6×12, 7×7, and 6×6 $\vec{k}_{||}$ points were respectively sampled to obtain their final energies. The total energies of the six SAM models were minimized until the maximum ionic forces were smaller than 25 meV/Å.

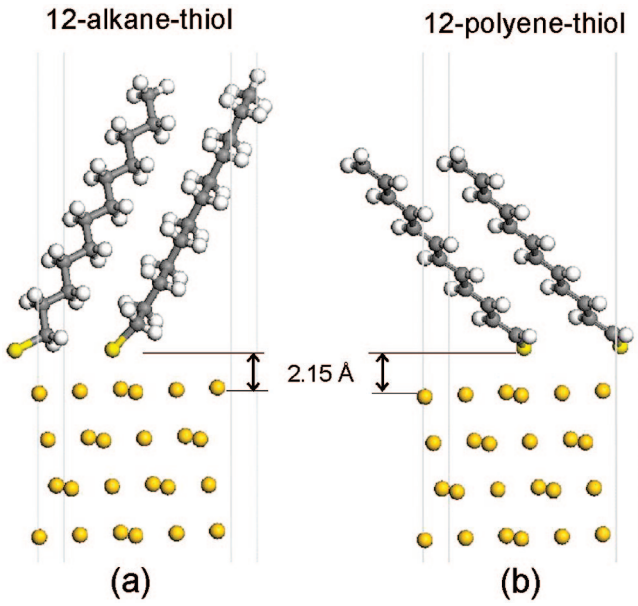

Figure 3. Structures of (a) $(2\sqrt{3} \times \sqrt{3})$R30° 12-alkane-thiolate and (b) $(2\sqrt{3} \times \sqrt{3})$R30° 12-polyene-thiolate SAMs.

Formation energies and tilt angles are presented in Table 3 together with the root-mean-square deviation of atomic positions in each case. We see that the FF-derived structures compare well with those that are further optimized within the PBE-GGA. More importantly, we confirm that $(\sqrt{3} \times \sqrt{3})$R30° is the optimal packing density with DFT.

Two significant differences between the FF and DFT results are

(1) the relative stability of the alkane and polyene SAMs is reversed

(2) PBE leads to a much smaller energy difference between the $(\sqrt{3} \times \sqrt{3})$R30° and 2×2 Au(111) cell-based structures than the FF. However, these packing interactions are dominated by the London dispersion (van der Waals attraction) forces, which are known to be described poorly with these DFT methods. In contrast, the vdW part of the FF was fitted to experimental crystal structures. Thus, it may well be that the FF results are more accurate. In any case, these differences do not affect the calculations of the current−voltage characteristics considered in section 4.

4. Current−Voltage Characteristics from Matrix Green's Function Calculations

Using the device structures based on the $(2\sqrt{3} \times \sqrt{3})$R30° cell (section 2), we performed MGF calculations[30] to compute the transmission function T and the density of states (DOS). Since we have to deal with many device models, and are mainly interested in the relative differences between their characteristics, we introduced approximations not made in our previous studies[3,4,31] as follows:

(i) The first part of the MGF calculation consists of three DFT calculations: one for the main 2D device model (bottom Au electrode + alkane/polyene-(di)thiolates + top Au electrode) and two additional ones for the 3D crystal structures corresponding to the bottom and top Au electrodes. It would be proper to base the latter bulk 3D models on the ideal perfect crystal structures, but the Au electrode atoms in our SAM models are perturbed only insignificantly from the perfect crystalline geometry, with very small Au relaxations. Thus, we

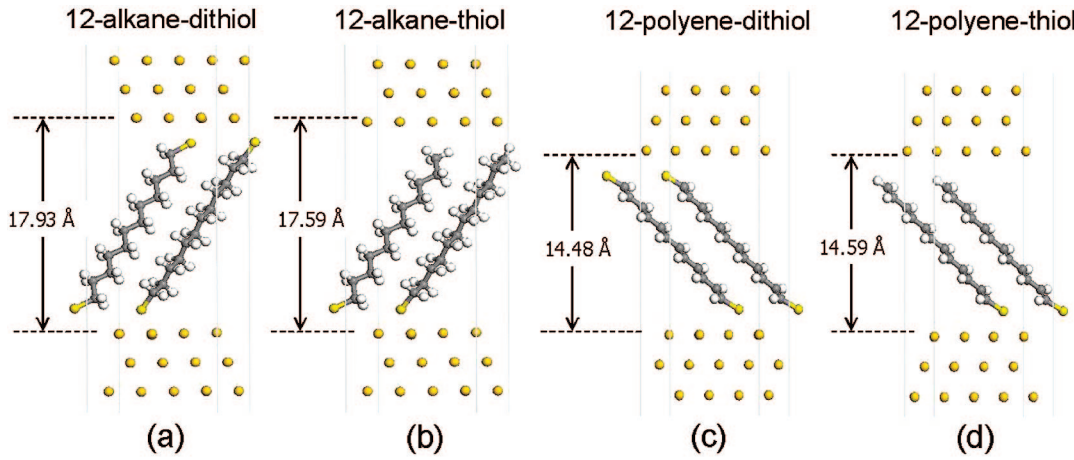

Figure 4. Structures of (a) $(2\sqrt{3} \times \sqrt{3})$R30° 12-alkane-dithiolate and (b) corresponding 12-alkane-thiolate SAM devices. Structures of (c) $(2\sqrt{3} \times \sqrt{3})$R30° 12-polyene-dithiolate and (d) corresponding 12-polyene-thiolate SAM devices.

TABLE 2: Tilt Angles and Formation Energies of 12-Polyene-thiolate SAMs for Various Packing Densities

system	number of surface Au atoms/chain	area per molecule (Å^2)	tilt angle (deg)	total energy (kcal/mol)	energy of gold (kcal/mol)	energy of molecule (kcal/mol)	formation energy (kcal/mol)
single 12-polyene chain	1	7.20	0	165.38	−86.18	5.93	245.62
	2	14.41	2.3	−195.04	−172.39	5.93	−28.58
	3	21.61	**48.0**	−313.69	−234.11	5.93	**−85.51**
	4	28.81	57.4	−392.15	−344.83	5.93	−53.25
	6	43.22	70.2	−561.51	−517.29	5.93	−50.16
	9	64.83	78.1	−811.86	−775.91	5.93	−41.88
double 12-polyene chains	1	14.41	0	132.55	−172.39	5.93	146.54
	2	28.81	1.1	−405.87	−344.83	5.93	−36.45
	3	43.21	**48.2**	−624.21	−456.41	5.93	**−89.83**
	4	57.63	57.7	−779.71	−689.70	5.93	−50.94
	6	86.44	69.7	−1117.07	−1031.25	5.93	−48.84

based the Au electrode parts directly on the structures from the FF-relaxed device models. One measure to quantify the accuracy of this approximation is to determine the "numerical" gap produced in the bulk 3D calculations.[4] Usually, we find a gap of $\sim 10^{-4}$ eV or less from calculations using the perfect crystal geometry. Using the electrode atom configurations directly taken from the SAM models, we still find a gap of 10^{-2} eV. This is sufficiently small to ensure an accurate alignment of energy levels from three DFT calculations.[4]

(ii) The second part of the MGF calculation is to generate the surface Green's functions and calculate transmission factors. Here, we simplified by using only the actual molecules as the scattering region. We could increase the accuracy of the calculation by incorporating extra layers of electrode atoms within the scattering region.[3,31] We did not do so here because the resulting changes were found to be rather small for our purpose of comparing different molecular structures.

After calculating the transmission function, we obtained the current−voltage ($I-V$) characteristics via the Landauer−Büttiker formula

$$I(V) = \frac{2e}{h}\int_{\mu_1}^{\mu_2} \mathrm{d}E T(E,V)[f(E-\mu_1) - f(E-\mu_2)] \quad (2)$$

where μ_1 and μ_2 are the chemical potentials of the two electrodes and f is the Fermi−Dirac distribution function. Since we are interested in the low-bias regime $I-V$ characteristics, we carried out non-self-consistent MGF calculations based on the zero-bias DFT output and used the approximation $T(E,V) \approx T(E,0)$ to obtain the $I-V$ curves. Here, we also assumed a symmetric distribution of the bias voltages across the bottom and top contacts, $\mu_1 = E_F + 0.5\ eV$ and $\mu_2 = E_F - 0.5\ eV$, where E_F is the Fermi energy of the system. This should be a good approximation for the dithiolate cases but is less accurate for the monothiolate cases. However, since the systems considered here have rather flat transmissions around E_F, we expect this to be a reliable approximation (at least for low-bias voltage regimes of our interest). Further details on the theoretical and numerical issues of our MGF implementation were presented elsewhere.[3,4,31]

4.1. Alkane Case. The transmission functions calculated for the *n*-alkane-dithiolate and *n*-alkane-thiolate junctions are shown in Figure 5a and b, and the resulting $I-V$ curves are shown in Figure 6a and b, respectively. As expected for coherent nonresonant tunneling through insulating materials,[32,33] we observe an exponential decay of current (an exponential increase of resistance) with respect to chain length

$$R = R_0 \exp(\beta_n n) \quad (3)$$

where R_0 is a reference contact resistance, n is the number of carbon repeat units, and β_n is the decay coefficient per methylene unit. Semilog plots of tunneling resistance per molecule at 0.1 V in units of R_K ($=h/e^2 = 25812.8\ \Omega$) versus the number of methylene units for the alkane-dithiolates and alkane-thiolates are shown in Figure 7a.

We obtain $\beta_n = 0.82$ for the alkane-monothiolates, or expressing this in units of inverse length $\beta_d = 0.80$ Å^{-1} (with $R^2 = 1.00$). Representative experimental values from the literature are the following: $\beta_d = 0.85$ Å^{-1} (Weber et al.[34]), $\beta_d = 0.89$ Å^{-1} (Slowinski et al.[35]), $\beta_d = 0.88$ Å^{-1} (Frisbie et al.[36]),

TABLE 3: Tilt Angles and Formation Energies of 8-Alkane/Polyene-thiolate SAMs for Several Packing Densities Obtained from PBE DFT Calculations[a]

system	number of surface Au atoms/chain	area/molecule (Å^2)	tilt angle (deg)	formation energy (kcal/mol)	rms deviation (Å)
8-alkane	2	14.41	32.5	82.43	0.236
	3	21.61	**35.6**	**−42.53**	0.531
	4	28.81	51.0	−40.00	0.281
8-polyene	2	14.41	9.0	7.71	0.311
	3	21.61	**45.5**	**−25.08**	0.652
	4	28.81	57.2	−23.88	0.420

[a] Root-mean-square (RMS) deviations of atomic positions between the initial FF-generated structures and the final PBE DFT-optimized structures are also shown together.

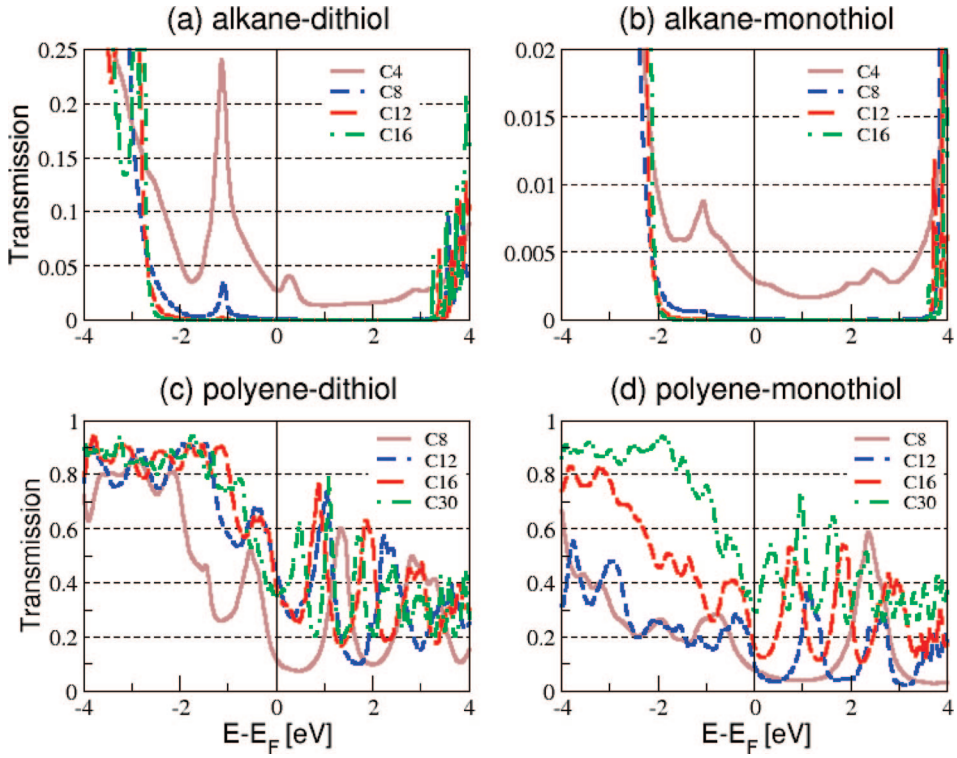

Figure 5. Transmission function per molecule of (a) alkane-dithiolate, (b) alkane-thiolate, (c) polyene-dithiolate, and (d) polyene-thiolate SAMs.

$\beta_n = 0.8$ (Cui et al.[37]), and $\beta_d = 0.83$ Å^{-1} (Lee et al.[38]). In the above evaluation of β_d, we chose d to be the total distance between the surface layer Au atoms on each electrode. If instead we choose d to be the distance between the terminal C or S atoms of the molecule, we obtain a reduced value of $\beta_d = 0.71-0.74$ Å^{-1}, depending on the definition of "molecule length" (e.g., bottom S to top C distance, bottom C−top C distance, etc.). Because of the ambiguity of defining the "distance" d,[31] especially when the molecules are tilted as in the SAM configuration, we refer only to β_n in the following.

For the alkane-dithiolate case, we obtained $\beta_n = 0.88$ ($R^2 = 1.00$). This can be compared to the value $\beta_n = 0.90$ obtained for the stretched single-molecule case.[31] This good agreement between the single-molecule and SAM cases is due to the negligible effect of molecular tilting and monolayer packing on the charge transport characteristics of alkane-based devices.[4]

Finally, the effective contact resistances R_0 for the dithiolate and monothiolate contacts are 12.69 and 176.69 kΩ, respectively. Thus, the ratio of the resistance of the monothiolate chains compared to the dithiolate chains is R_0(mono)/R_0(di) = 12.5. This shows the significant effect of having a vdW or physisorption contact at one end for the monothiolate. This ratio agrees qualitatively with other studies[39] that found alkane-dithiolate junctions to have contact resistances 1−2 orders of magnitude smaller than that of alkane-thiolate junctions.

4.2. Polyene Case. Polyene SAMs have not yet been reported experimentally, perhaps because the conjugated double bonds are sensitive to oxidation. Bulk polyacetylene films have been synthesized, but all have significant disorder. It has been shown that increased disorder of the in-plane alignment of fine fibrils in ultrathin polyacetylene films leads to a decrease in electrical conductivity from those expected of an ordered system.[40] As a result, experimental $I-V$ data is not yet available for polyene SAMs. We will now suggest that polyene SAMs would have particularly interesting $I-V$ properties, making their synthesis most desirable.

The predicted tunneling transmission as a function of voltage is shown in Figure 5c for the *n*-polyene-dithiolate junction and in Figure 5d for the *n*-polyene-thiolate junction. The resulting $I-V$ curves are shown in Figure 6c and d. *The most notable result is that we find no increase in resistance for polyenes with increased chain length,* as shown in Figure 7b. That is, *the polyene chains behave as metals.* This is in contrast to bulk polyacetylenes that are well-known to be semiconductors, becoming conductors only with doping.[41−43]

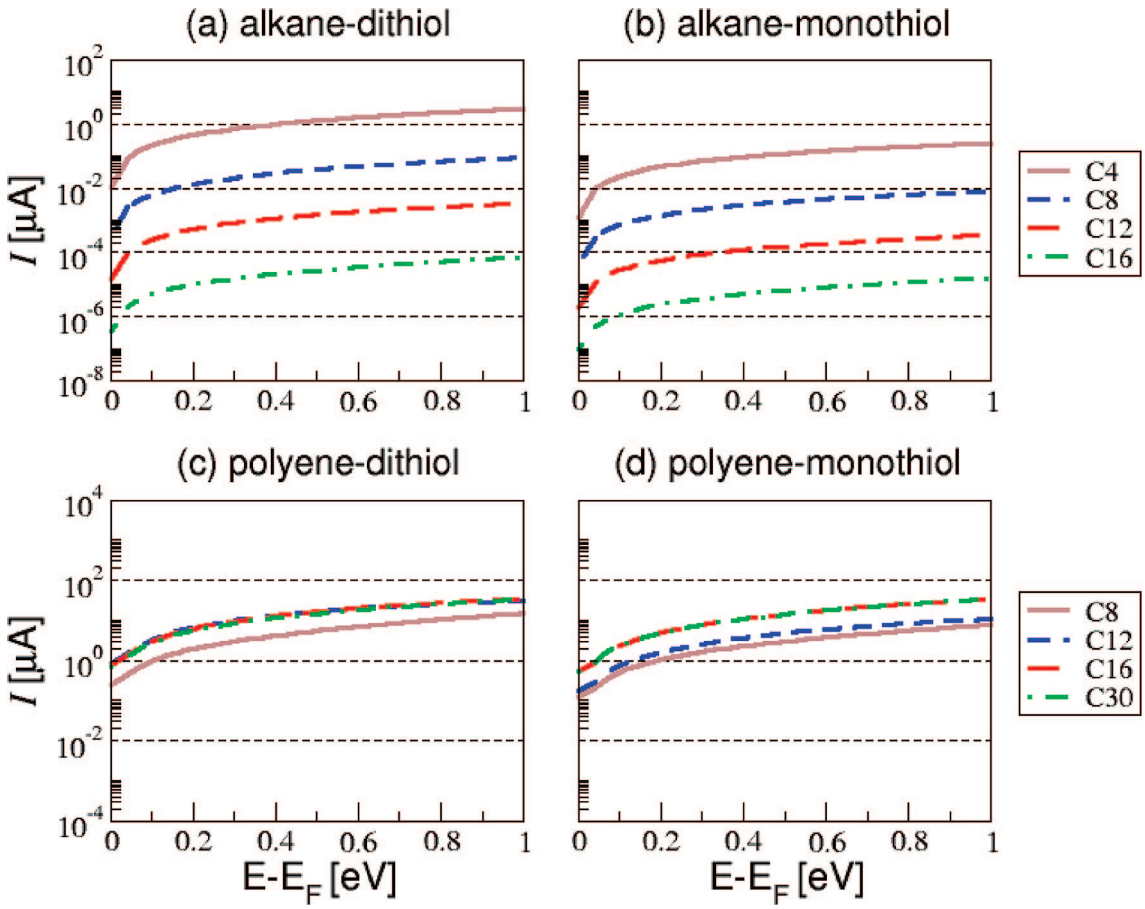

Figure 6. Current (per molecule)−voltage curves shown on a semilogarithmic scale for the (a) alkane-dithiolate, (b) alkane-thiolate, (c) polyene-dithiolate, and (d) polyene-thiolate SAM junctions. Parts a and b show the exponential decay of the tunneling current for the alkane SAMs and show that the junctions with two dithiolate contacts have currents a factor of ~12 larger than those with monothiolates. Parts c and d show no systematic length dependence in current and a much smaller contact dependence for the polyene SAMs.

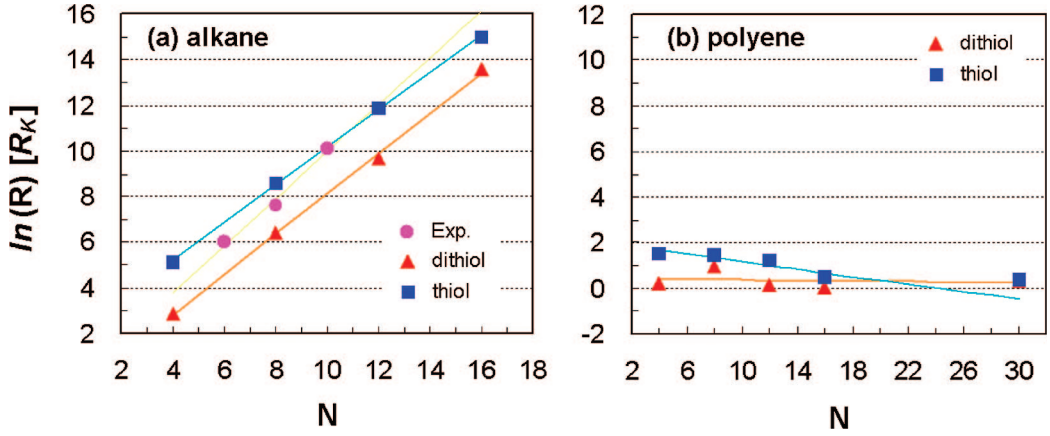

Figure 7. Dependence of junction resistance on the molecular length for the (a) alkane and (b) polyene SAMs. Lines are linear fits. The polyalkane SAMs show exponentially increasing resistance, with $\beta_n = 0.82$ for monothiolates and $\beta_n = 0.88$ for dithiolates. The experimental data for the alkane case are from the STM measurements of single dithiolate molecules by Xu et al.[44] The polyene-based SAMs show no systematic length dependence.

We find that the effective contact resistances R_0 for the polyene-dithiolate and polyene-monothiolate contacts are 39.07 and 141.73 kΩ, respectively. This magnitude of contact resistances for the polyene junctions are similar to those for the alkane junctions, but the ratio R_0(mono)/R_0(di) = 2.8 is much smaller than the value of 12.5 for the alkane case. In the next section, we will analyze the physical origin of the contrasting charge transport behavior of alkane and polyene SAMs.

4.3. Discussion: Comparison of Alkane and Polyene *I*−*V* Data. We now analyze the characteristic conductance scaling with the molecule length in alkane chains (section 4.1) as well as the lack of length dependence in polyene chains (section 4.2) by analyzing DOS projected onto the S linkage atoms and the remaining molecular cores. The PDOS curves for the alkane and polyene chains are presented in Figures 8 and 9, respectively.

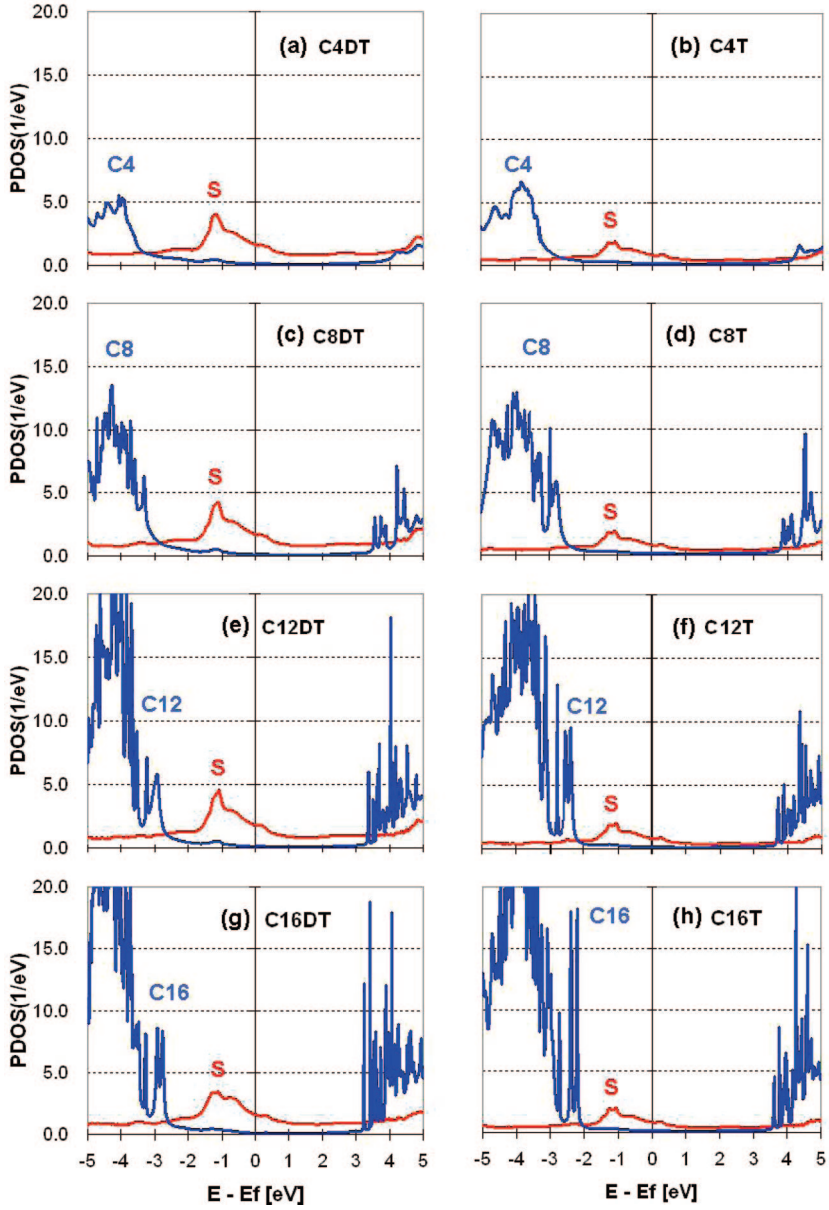

Figure 8. PDOS per molecule of thiolates (red lines) and alkane cores (blue lines) for the *n*-alkane-thiolate (T) and *n*-alkane-dithiolate (DT) SAMs. This shows that the HOMO is dominated by S character, with large band gaps for alkane chains.

First, we consider the alkane case (Figure 8). We observe that the DOS around E_F is dominated by the S PDOS with peaks at $\sim E_F - 1.3$ eV, which makes it the highest occupied molecular orbital (HOMO) of the entire molecule. The S PDOS of dithiolate (monothiolate) models is more or less constant throughout all the dithiolate (monothiolate) systems, which indicates that the local S−Au linkage chemistry is almost identical in all of the models. We also find that the S PDOS of dithiolate models is about 2 times larger than that of the monothiolate models.

Compared with the S PDOS, the HOMO of the alkane core is about 3.0 eV below E_F and the lowest unoccupied molecular orbital (LUMO) PDOS of the alkane core lies at about 3.0 eV above E_F. Due to this large HOMO−LUMO gap of the alkane cores, the increase of chain length increases only the PDOS in the energy region < -3 eV and $> +3$ eV, with no effect on the transmission channels around E_F. Because the dominant PDOS contribution at E_F resulted from the S linkage atoms and the molecular core simply acts as a tunneling barrier, the conductance of alkane-based junctions exponentially decreases with respect to the molecular length and the contact resistance depends critically on whether there are one or two thiolate bridges (Figures 6a and b and 7a).

We next consider the polyene case (Figure 9). As in the alkane junctions, we find S PDOS contributions that are constant throughout all the dithiolate (thiolated) junctions with peaks at $\sim E_F - 1.5$ eV. The difference is that the HOMOs of the entire polyalkane-dithiolate and polyalkane-thiolate junctions are derived from the S atoms, whereas for the polyene cases we find that the HOMOs and LUMOs originate from the polyene cores which have significant contributions to the PDOS near E_F. In particular, we find that the polyene HOMOs are fixed at $\sim E_F - 0.5$ eV, while the location of LUMOs moves downward from $\sim E_F + 2.0$ eV for the 4-polyene junctions to $\sim E_F + 0.5$ eV for the 30-polyene junctions. The decreasing HOMO−LUMO gap increases the polyene PDOS near E_F as the chain length increases. This increasing number of charge conductance channels through molecular cores around E_F cancels the effect of the increasing distance that the tunneling electrons must travel, explaining the lack of length dependence of contact

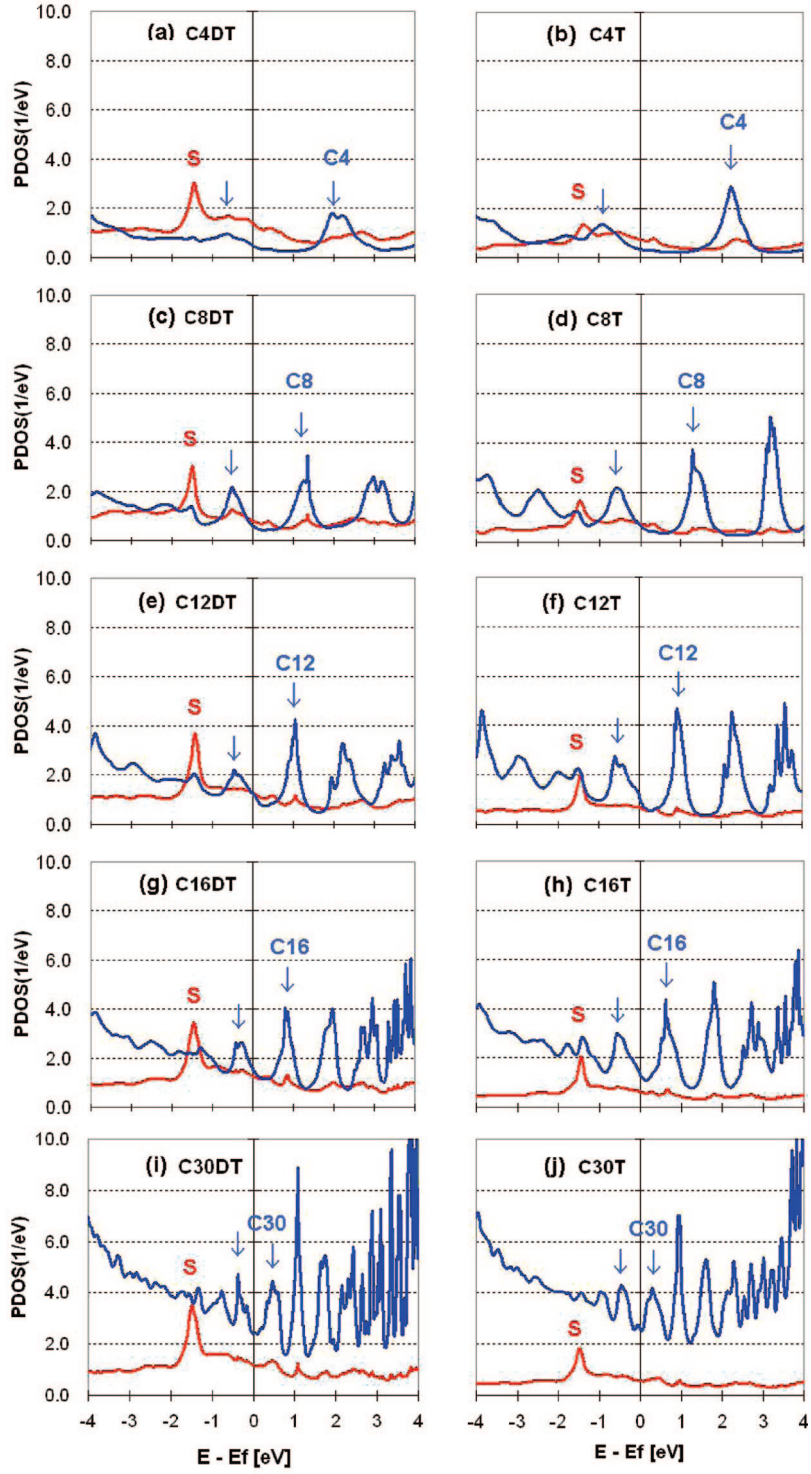

Figure 9. PDOS per molecule of thiolates (red lines) and polyene cores (blue lines) for the *n*-polyene-thiolates (T) and *n*-polyene-dithiolate (DT) SAMs. Here, the HOMOs and LUMOs are dominated by the polyene molecular cores. The HOMO−LUMO gap decreases with *n*, resulting in an increase of the DOS near E_F with increasing *n*.

resistance in nanoscale polyene-based junctions. The dominance of polyene PDOS compared to thiolate PDOS furthermore indicates a strong coupling of molecular cores to the electrodes, which results in the much smaller thiolate/dithiolate ratio of the junction resistance in the polyene case.

5. Summary

In this work, we studied the packing configuration and transmission properties of *n*-alkane-thiolate, *n*-alkane-dithiolate, *n*-polyene-thiolate, and *n*-polyene-dithiolate monolayer devices using QM DFT-MGF methods supplemented with classical FF based partly on QM.

We find that the optimal packing for the alkane-thiolate SAMs has the $(\sqrt{3} \times \sqrt{3})R30°$ packing with a 2×1 superlattice structure corresponding to the herringbone packing of adjacent chains. This is in good agreement with experiments,[8] validating our computational approach.

For the polyene-thiolate SAMs, we obtained the same ($\sqrt{3} \times \sqrt{3}$)R30° packing density as for the alkanes but with a 1×1 superlattice structure corresponding to the parallel arrangement of polyene chains. We are not aware of any experimental data with which to compare these results.

The central focus of this study was the SAM charge transport properties of the polyene SAMs, which have not yet been studied experimentally. Most surprising is the predicted excellent conductance properties, in which there is no length-dependent decay in current even up to 30-polyene chain length. In addition, the dependence of contact resistance on the number of thiolate contacts is small, increasing only by a factor of ~2.8 upon forming the second electrode thiolate covalent bond.

For the *n*-alkane devices, we find the well-known exponential decay with a decay constant of $\beta_n = 0.82$ for the monothiolate junctions and $\beta_n = 0.88$ for the dithiolate junctions. This is in good qualitative agreement with other experimental and theoretical investigations. The resistance of monothiolate junctions was found to be ~12.5 times larger than that of dithiolate counterparts.

To explain this difference in transmission characteristics between the alkane-(di)thiolate and polyene-(di)thiolate junctions, we examined the PDOS of molecular cores (alkanes and polyenes) and thiolate contacts. For the alkane case, the DOS around E_F was dominated by S HOMO PDOS with a negligible PDOS from the molecular core. On the other hand, for the polyene case, we found polyene-originated HOMOs and LUMOs, and significant molecular core (polyene) PDOS around E_F that increases with the chain length. This unexpected lack of length dependence in the resistance of nanoscale polyene SAM junctions might be tested experimentally, which could prove to be a useful ingredient for the future development of molecular electronics.

Acknowledgment. C.G. was supported primarily by the MRSEC Program of the National Science Foundation under Award No. DMR-0080065 (Caltech). S.S.J. and W.A.G. were supported by NSF CCF-0524490, MARCO FENA, and Intel Component Research. The computational facilities of the MSC were also supported by ONR-DURIP and ARO-DURIP. Y.-H.K. was supported by the Korea Research Foundation (Grant No. KRF-2007-331-C00077) and the Korea Science and Engineering Foundation (Grant No. 2008-02807). Most calculations were performed by using the supercomputing resource of the Korea Institute of Science and Technology (KISTI).

References and Notes

(1) Heath, J. R.; Ratner, M. A. *Phys. Today* **2003**, *56 May*, 43.
(2) Lindsay, S. M. *Faraday Discuss.* **2006**, *131*, 403.
(3) Kim, Y.-H.; Jang, S. S.; Goddard, W. A., III. *J. Chem. Phys.* **2005**, *122*, 244703.
(4) Kim, Y.-H.; Tahir-Kheli, J.; Schultz, P. A.; Goddard, W. A., III. *Phys. Rev. B* **2006**, *73*, 235419.
(5) Kim, Y.-H.; Jang, S. S.; Jang, Y. H.; Goddard, W. A., III. *Phys. Rev. Lett.* **2005**, *94*, 156801.
(6) Kim, Y.-H.; Jang, S. S.; Goddard, W. A., III. *Appl. Rev. Lett.* **2006**, *88*, 16312.
(7) Kim, Y.-H.; Goddard, W. A., III. *J. Phys. Chem. C* **2007**, *111*, 4831.
(8) Love, J. C.; Estroff, L. A.; Kriebel, J. K.; Nuzzo, R. G.; Whitesides, G. M. *Chem. Rev.* **2005**, *105*, 1103.
(9) Mayo, S. L.; Olafson, B. D.; Goddard, W. A., III. *J. Phys. Chem.* **1990**, *94*, 8897.
(10) Jang, S. S.; Jang, Y. H.; Kim, Y.-H.; Goddard, W. A., III; Flood, A. H.; Laursen, B. W.; Tseng, H.-R.; Stoddart, J. F.; Jeppesen, J. O.; Choi, J. W.; Steuerman, D. W.; DeIonno, E.; Heath, J. R. *J. Am. Chem. Soc.* **2005**, *127*, 1563.
(11) Rappé, A. K.; Goddard, W. A., III. *J. Phys. Chem.* **1991**, *95*, 3358.
(12) Porter, M.; Bright, T.; Allara, D.; Chidsey, C. *J. Am. Chem. Soc.* **1987**, *109*, 3559.
(13) Fenter, P.; Eberhardt, A.; Liang, K. S.; Eisenberger, P. *J. Chem. Phys.* **1997**, *106*, 1600.
(14) Torrelles, X.; Barrena, E.; Munuera, C.; Rius, J.; Ferrer, S.; Ocal, C. *Langmuir* **2004**, *20*, 9396.
(15) Gerdy, J. J.; Goodard, W. A., III. *J. Am. Chem. Soc.* **1996**, *118*, 3233.
(16) Vemparala, S.; Karki, B.; Kalia, R. K.; Nakano, A.; Vashishta, P. *J. Chem. Phys.* **2004**, *121*, 4323.
(17) Fenter, P.; Eberhardt, A.; Eisenberger, P. *Science* **1994**, *266*, 1216.
(18) Vargas, M.; Giannozzi, P.; Selloni, A.; Scoles, G. *J. Phys. Chem. B* **2001**, *105*, 9509.
(19) Fischer, D.; Curioni, A.; Andreoni, W. *Langmuir* **2003**, *19*, 3567.
(20) Maksymovych, P.; Sorescu, D. C.; Yates, J. T. *Phys. Rev. Lett.* **2006**, *97*, 146103.
(21) Mazzarello, R.; Cossaro, A.; Verdini, A.; Rousseau, R.; Casalis, L.; Danisman, M. F.; Floreano, L.; Scandolo, S.; Morgante, A.; Scoles, G. *Phys. Rev. Lett.* **2007**, *98*, 016102.
(22) Camillone, N.; Chidsey, C.; Liu, G.; Scoles, G. *J. Chem. Phys.* **1993**, *98*, 3503.
(23) Poirier, G. E.; Tarlov, M. J. *Langmuir* **1994**, *10*, 2853.
(24) Torrelles, X.; Vericat, C.; Vela, M. E.; Fonticelli, M. H.; Millone, M. A. D.; Felici, R.; Lee, T. L.; Zegenhagen, J.; Munõz, G.; Martín-Gago, J. A.; Salvarezza, R. C. *J. Phys. Chem. B* **2006**, *110*, 5586.
(25) Yu, M.; Bovet, N.; Satterley, C. J.; Bengió, S.; Lovelock, K. R. J.; Milligan, P. K.; Jones, R. G.; Woodruff, D. P.; Dhanak, V. *Phys. Rev. Lett.* **2006**, *97*, 166102.
(26) Akaishi, T.; Miyasaka, K.; Ishikawa, K.; Shirakawa, H.; Ikeda, S. *J. Polym. Sci.* **1980**, *18*, 745.
(27) Schultz, P. SeqQuest code project (Sandia National Laboratories), http://dft.sandia.gov/Quest.
(28) Perdew, J. P.; Burke, K.; Ernzerhof, M. *Phys. Rev. Lett.* **1996**, *77*, 3865.
(29) Fuchs, M.; Scheffler, M. *Comput. Phys. Commun.* **1999**, *119*, 67.
(30) Datta, S. *Quantum Transport: Atom to Transistor*; Cambridge University Press: Cambridge, U.K., 2005.
(31) Kim, Y.-H. *J. Kor. Phys. Soc.* **2008**, *52*, 1181.
(32) Tomfohr, J. K.; Sankey, O. F. *Phys. Rev. B* **2002**, *65*, 245105.
(33) Kaun, C. C.; Guo, H. *Nano Lett.* **2003**, *3*, 1521.
(34) Weber, K.; Hockett, L.; Creager, S. *J. Phys. Chem. B* **1997**, *101*, 8286.
(35) Slowinski, K.; Chamberlain, R. V.; Miller, C. J.; Majda, M. *J. Am. Chem. Soc.* **1997**, *119*, 11910.
(36) Engelkes, V. B.; Beebe, J. M.; Frisbie, C. D. *J. Am. Chem. Soc.* **2004**, *126*, 14827.
(37) Cui, X. D.; Zarate, X.; Tomfohr, J.; Sankey, O. F.; Primak, A.; Moore, A. L.; Moore, T. A.; Gust, D.; Harris, G.; Lindsay, S. M. *Nanotechnology* **2002**, *13*, 5.
(38) Lee, T.; Wang, W.; Reed, M. A. *J. Phys. Chem. B* **2004**, *108*, 8742.
(39) Kaun, C.-C.; Guo, H. *Nano Lett.* **2003**, *3*, 1521.
(40) Liang, T. S.; Akagi, K.; Shirakawa, H. *Synth. Met.* **1999**, *101*, 67.
(41) Heeger, A. J. *Rev. Mod. Phys.* **2001**, *73*, 681.
(42) MacDiarmid, A. G. *Rev. Mod. Phys.* **2001**, *73*, 701.
(43) Shirakawa, H. *Rev. Mod. Phys.* **2001**, *73*, 713.
(44) Xu, B.; Tao, N. J. *Science* **2003**, *301*, 1221.

JP061759L